COMMUNICATION

AgPd nanoparticles supported on zeolitic imidazolate framework derived N-doped porous carbon as an efficient catalyst for formic acid dehydrogenation†
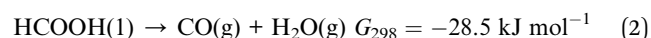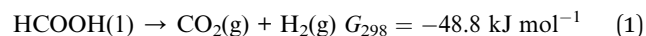
Cheng Feng, Yunhui Hao, Li Zhang, Ningzhao Shang, Shutao Gao,* Zhi Wang and Chun Wang*

Formic acid (FA) has tremendous potential as a safe and convenient source of hydrogen for renewable energy storage, but controlled and efficient dehydrogenation of FA by a robust solid catalyst constitutes a major challenge. In this report, a metal nanoparticle functionalized zeolitic imidazolate framework (ZIF) derived N-decorated nanoporous carbon (NPC) support was fabricated and used as an efficient FA decomposition catalyst for the first time. The resultant AgPd@NPC catalyst exhibited 100% H_2 selectivity and high catalytic activity (TOF = 936 h^{-1}) toward the dehydrogenation of formic acid at 353 K. The synergetic interaction between the metal nanoparticles and NPC greatly enhances the catalytic performance of the as-prepared catalyst.

Introduction

With the increased consumption of fossil fuel energy and growing environmental contamination, the exploitation of clean, renewable and sustainable energies is highly desirable. Among the various alternative energy strategies, hydrogen has been considered as an environmentally attractive energy carrier for electricity generation in a fuel cell due to water being the only byproduct.[1] However, storage and distribution of hydrogen in a safe and efficient way still remain challenging issues.[2] Recently, formic acid (FA), one of the major products of biomass processing and catalytic CO_2 hydrogenation with a high H_2 content (4.4%), has been considered as a potential liquid storage material capable of releasing H_2 under mild conditions *via* catalytic decomposition. Formic acid as a liquid hydrogen fuel possesses the potential advantages of utilizing the current liquid-based

College of Sciences, Agricultural University of Hebei, Baoding 071001, Hebei, P. R. China. E-mail: chunwang69@126.com; gst824@163.com; Fax: +86-312-7528292

† Electronic supplementary information (ESI) available: Calculation method of TOF, the metal mass content in the catalysts, the recyclability of the catalyst, GC analysis of the evolved gas from aqueous FA solution. See DOI: 10.1039/c5ra04157k

distribution infrastructure. Moreover, FA is a promising candidate as a safe and convenient H_2 carrier for portable hydrogen storage applications due to its nontoxicity, high stability, easy recharging ability, and high energy density.[1] The decomposition of formic acid follows two principal pathways: the dehydrogenation pathway to form H_2 and CO_2 (eqn (1)), and the dehydration pathway to form H_2O and CO (eqn (2)).

$$HCOOH(l) \rightarrow CO_2(g) + H_2(g) \quad G_{298} = -48.8 \text{ kJ mol}^{-1} \quad (1)$$

$$HCOOH(l) \rightarrow CO(g) + H_2O(g) \quad G_{298} = -28.5 \text{ kJ mol}^{-1} \quad (2)$$

Reaction (2) is the undesirable pathway as CO is highly toxic to fuel cell catalysts, so it should be strictly controlled.[2] The reactivity and selectivity of these two pathways are strongly dependent on the catalysts used, pH of the medium and the reaction temperature. To achieve efficient FA dehydrogenation, the development of efficient and cost-effective catalysts is highly desirable.

Up to now, both homogeneous and heterogeneous catalysts for catalytic FA dehydrogenation have been developed.[3–7] However, the separation and reusability issues associated with homogeneous catalysts hinder their use in practical applications. To circumvent these issues, the development of efficient heterogeneous catalysts has received considerable attention in recent years.[8–13] Pt, Au and Pd are the primary catalytic metals used in heterogeneous catalysis.[1] Among them, Pt and Au are much more expensive than Pd. Furthermore, Pt without surface modification or alloying tends to suffer severe CO poisoning from FA dehydration, and for Au, a high catalytic activity can only be obtained on subnanometric clusters supported on selected metal oxides, which is not trival in scale-up synthesis.[8] In this connection, Pd-based nanocatalysts are most attractive for practical hydrogen production from FA decomposition. In recent years, heterogeneous catalysts containing Pd, including Ag–Pd core–shell,[10] monodisperse AgPd alloy nanoparticles[11] and metal organic frameworks (MOF)

materials,[12,13] have been studied for catalytic dehydrogenation of formic acid. It has been demonstrated that the type of the support, the dispersity of the metal nanoparticles and the synergetic interaction between the metal and support play a key role for the catalytic performance of the nanocatalysts and the kinetic properties of FA dehydrogenation.[2]

Carbons, especially nanoporous carbon materials, have been the most important and traditionally support for heterogeneous catalyst due to their high specific surface area and large pore volume in combination with excellent thermal, chemical and mechanical stability. It is well known that the coupling of nitrogen element into the carbon materials is favorable for the stabilization of highly dispersed metal nanoparticles.[14,15] In general, N-doped porous carbons (NPC) could be synthesized via amine etc. grafting on the carbon matrix. However, the post synthetic incorporation method not only blocks pores but also suffers from leaching and instability in any subsequent regeneration step. Another synthesis strategy of NPC is high temperature pyrolysis of heteroatom-containing precursors. An ideal starting material is the one that can act as template, carbon precursor and nitrogen source. In that direction, zeolitic imidazolate framework (ZIF) resulting from periodically arranged organometallic complexes, which has the advantages of high specific surface area and porosity, chemical tunability, and well-defined pore structure, might be the promising precursors and hard templates for in situ casting of NPC since the organic ligands contain various other types of atoms (N, O, etc.) other than carbon.[16] So far, several ZIFs, such as ZIF-67 (ref. 17, 18), ZIF-7 (ref. 19) and ZIF-8 (ref. 20) have been demonstrated as precursors to construct nanoporous carbon materials.

In this report, AgPd nanoparticles functionalized with ZIF-8 ($Zn(MeIM)_2$, MeIM = 2-methylimidazole) derived NPC would be fabricated and used as an efficient FA decomposition catalyst for the first time. This study demonstrated that the metal nanoparticles supported on metal–organic frameworks-derived NPC materials could act as promising catalysts for the dehydrogenation of formic acid.

Experimental

Chemicals

Palladium chloride ($PdCl_2$) and MeIM were all obtained from Aladdin Reagent Limited Company. Formic acid (FA), sodium formate (SF), concentrated HCl, $Zn(NO_3)_2 \cdot 6H_2O$, $AgNO_3$, NaOH, N,N-dimethyl formamide (DMF), methanol and other reagents were of analytical grade. All the chemicals were used as received without any purification. High-purity argon and distilled water were used in all experiments.

Physical characterizations

The size and morphology of the nanoparticles were observed by transmission electron microscopy (TEM) using a JEOL model JEM-2011(HR) at 200 kV. The XRD patterns of the samples were recorded with a Rigaku D/max 2500 X-ray diffractometer using Cu Kα radiation (40 kV, 150 mA) in the range $2\theta = 10–90°$. X-ray photoelectron spectroscopy (XPS) was performed with a PHI 1600 spectroscope using Mg Kα X-ray source for excitation. The surface area, total pore volume and pore size distribution of the samples were measured at 77 K by nitrogen adsorption using a APP V-Sorb 2600 Surface Area and Porosity Analyzer. The metal content of the materials was analyzed by a T.J.A. ICP-9000 type inductively coupled plasma atomic emission spectroscopy (ICP-AES) instrument. Detailed analyses for CO_2, H_2 and CO were performed on SP-2000 (Beijing Beifen Ruili Analytical Instrument CO., Ltd.). The H_2 and CO_2 compositions were measured by GC spectrum using TCD, while CO was measured by GC spectrum using FID-Methanator.

Synthesis of NPC

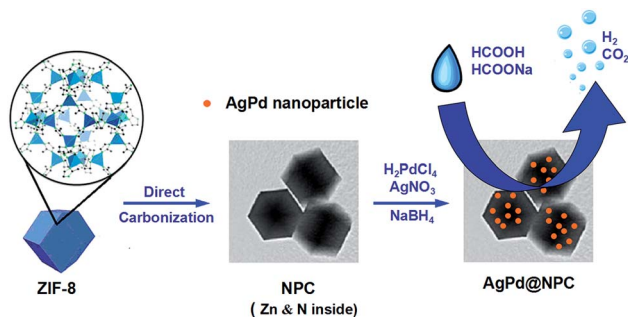ZIF-8 was prepared according to the procedure reported by Xu et al.[21] Briefly, a known quantity (744 mg, 25 mmol) of $Zn(NO_3)_2 \cdot 6H_2O$ was employed to obtain a mixture with Zn/MeIM/methanol in a molar ratio of approximately 1 : 1 : 500. The mixture was stirred for 1 h at ambient temperature. The turbid solution was allowed to stand for 12 h and the solid was recovered from the milky colloidal solution by centrifugation and washed with fresh methanol. Then the obtained ZIF-8 was dried under reduced pressure. For the synthesis of NPC, ZIF-8 nanocrystal (500 mg) was weighed in a ceramic boat and transferred into a quartz tube. The carbonization of the ZIF-8 was performed at 1073 K, 1173 K and 1273 K, respectively, for 10 h with an argon flow. The resulting product was denoted as ZIF8-C(n), where n represents the carbonization temperature (1073, 1173, 1273 K). The Zn residues in ZIF8-C(1073) were removed by the HCl solution (10 wt%) which is denoted ZIF8-C(1073)-HCl.

Synthesis of AgPd@NPC

For preparation of Ag_1Pd_4@ZIF8-C(1173), 95 mg of ZIF8-C(1173) was added to 5 mL solution of $AgNO_3$ (0.009 mmol) and newly prepared H_2PdCl_4 (0.036 mmol), and stirred for 24 h at 298 K to impregnate the metal salts. Then, ca. 0.4 mL of 2.0 mol L^{-1} NaOH solution was added into the above obtained solution with vigorous stirring, followed by an immediate addition of 10 mg $NaBH_4$ dissolved in 0.50 mL water. The mixture was stirred for 1 h at room temperature. After filtration, the obtained Ag_1Pd_4@ZIF8-C(1173) was dried under reduced pressure. The Ag_1Pd_4@ZIF8-C(1073), Ag_1Pd_4@ZIF8-C(1273) were fabricated with the same procedure except that ZIF8-C(1073), ZIF8-C(1273) were used, respectively. The Pd_5@ZIF8-C(1173), Ag_2Pd_3@ZIF8-C(1173), Ag_5@ZIF8-C(1173) catalysts were synthesized with the above procedure except that the theoretical mass ratios of Ag and Pd were 0 : 5, 2 : 3 and 5 : 0, respectively. (Scheme 1).

General procedure for dehydrogenation of formic acid reactions

The hydrogen production from FA–SF solution was carried out in a 10 mL round-bottomed flask, which was placed in an oil bath with magnetic stirrer at a preset temperature (333–353 K). A gas burette filled with water was connected to the reaction

Scheme 1 Schematic illustration for the preparation of AgPd@NPC.

Table 1 Textural properties of the $Ag_1Pd_4@ZIF8-C(n)$ determined by N_2 adsorption–desorption analysis

Sample	S_{BET}[a] ($m^2\ g^{-1}$)	V[b] ($cm^3\ g^{-1}$)	d_p[c] (nm)
$Ag_1Pd_4@ZIF8-C(1073)$	700	1.32	8.71
$Ag_1Pd_4@ZIF8-C(1173)$	466	0.63	6.31
$Ag_1Pd_4@ZIF8-C(1273)$	493	0.61	5.82

[a] BET surface area. [b] BJH cumulative desorption pore volume. [c] Mean pore diameter $= 4V/S_{BET}$.

flask to measure the volume of released gas. Firstly, 26.7 mg catalyst and 4 mL distilled water were placed in the round-bottomed flask. Then, the reaction started when 1.0 mL of the solution containing 1.25 mmol formic acid and 1.25 mmol sodium formate was injected into the mixture using a syringe. The molar ratios of Pd/formic acid were theoretically fixed at 0.01 for all the catalytic reactions. The volume of the evolved gas was monitored by recording the displacement of water in the gas burette.

Results and discussions

Characterization of the catalysts

For the preparation of NPC, the calcination temperature is crucial in determination of the textural properties and elemental composition of ZIF8-C(n). The pore properties of the $Ag_1Pd_4@ZIF8$-C(n) catalysts were investigated by nitrogen adsorption–desorption isotherms (Fig. 1). The steep increase in the adsorbed volume at low relative pressures reveals the presence of the micropores in the materials, and the following small slope observed at medium relative pressures as well as the desorption hysteresis denotes the existence of the mesopores (curves b and c) while the final almost vertical increase at the relative pressures near 1.0 points to the presence of macropores (curve a). Table 1 summarizes textural properties of the different annealing temperature catalysts characterized by N_2 adsorption–desorption analysis. As Table 1 shows
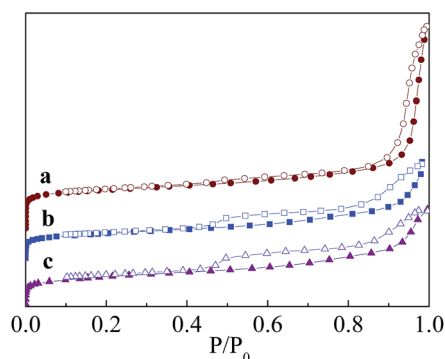
that the surface area and pore volume of $Ag_1Pd_4@ZIF8-C(1073)$, $Ag_1Pd_4@ZIF8-C(1173)$ and $Ag_1Pd_4@ZIF8-C(1273)$ catalysts were lower than that of the reference value for corresponding NPC,[20,21] which could be the result that a certain amount of metals was deposited in the pores of the NPC during the preparation process.

Fig. 2 displays the XRD pattern of the ZIF8-C(1173), $Pd_5@ZIF8-C(1173)$, $Ag_1Pd_4@ZIF8-C(1173)$, $Ag_2Pd_3@ZIF8$-C(1173), $Ag_5@ZIF8-C(1173)$, $Ag_1Pd_4@ZIF8-C(1073)$ and Ag_1-$Pd_4@ZIF8-C(1273)$. In general, the high annealing temperature allowed the evaporation of zinc (b.p. 1180 K),[22] so the zinc content decreased with increasing the carbonization temperature from 1073 to 1373 K. The zinc mass content in $Ag_1Pd_4@$ ZIF8-C(1073), $Ag_1Pd_4@ZIF8-C(1173)$ and $Ag_1Pd_4@ZIF8-C(1273)$ were 7.49%, 1.69%, and 0.55%, respectively, which were determined by ICP-AES. Comparing with the corresponding peaks of $Ag_1Pd_4@ZIF8-C(1073)$ and $Ag_1Pd_4@ZIF8-C(1273)$ between 38.03° and 40.10°, the peak of $Ag_1Pd_4@ZIF8-C(1173)$ was smaller and broader, which suggests that the well dispersion of AgPd alloy nanoparticles.[23,24] The metal mass content in the catalysts were determined by the ICP-AES, the results were shown in Table S1 (see ESI,†).

The XPS images of $Ag_1Pd_4@ZIF8-C(1173)$ were shown in Fig. 3, the $3d^{5/2}$ peak of Pd^0 appers at 335.9 eV,[10] the $3d^{5/2}$ peak of Ag^0 appers at 368.0 eV.[10] No obvious peaks of Ag^+ and Pd^{2+} observed, indicating the co-existence of both metals. The $2p^{2/3}$ peak of Zn^0 apper at 1022.2 eV which is slightly upshifted with respect to the reference value for Zn^0,[25] indicating that there is a

Fig. 1 N_2 adsorption–desorption isotherms of (a) $Ag_1Pd_4@ZIF8$-C(1073); (b) $Ag_1Pd_4@ZIF8-C(1173)$; (c) $Ag_1Pd_4@ZIF8-C(1273)$ at 77 K. Filled and open symbols represent adsorption and desorption branches, respectively.
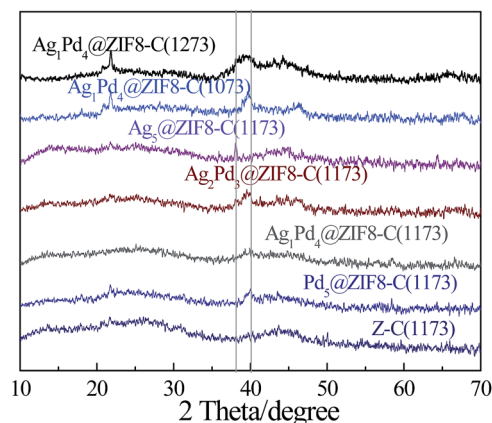

Fig. 2 Powder X-ray diffraction patterns of AgPd@ZIF8-C(n) and ZIF8-C(1173). The characteristic peak of Pd (111) is at $2\theta = 40.10°$, the characteristic peak of Ag (111) is at $2\theta = 38.03°$.

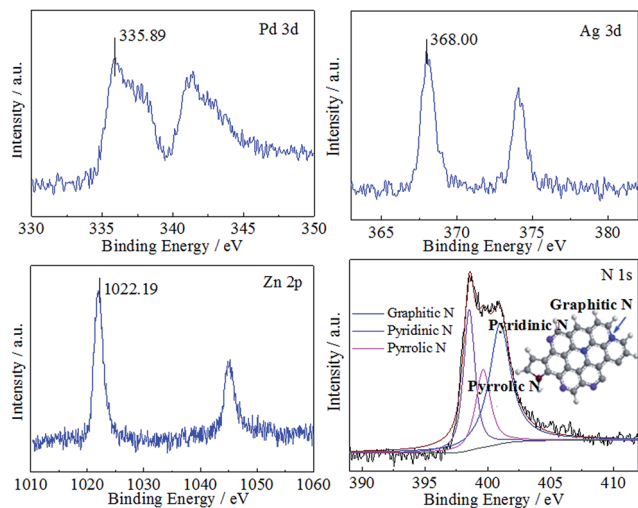**Fig. 3** XPS patterns of the Ag$_1$Pd$_4$@ZIF8-C(1173).

strong interaction between Zn and AgPd alloy. The electron transfer between Zn and AgPd alloy might lead to the change of Zn's binding energy. In the growth of ZIF-8 nanoporous carbons, MeIM ligands act as N source in the annealing process, thus forming nitrogen-doped carbon. The high resolution N 1s spectrum (Fig. 3) can be deconvoluted to three sub-peaks due to the spin orbit coupling, including pyridinic-N (398.5 eV), pyrrolic-N (399.7 eV) and graphitic-N (401.0 eV), which is a common characteristic for nitrogen-doped carbon materials.[26] In general, nitrogen in carbon texture is favorable for the stabilization of highly dispersed metal nanoparticles.

The morphologies of Ag$_1$Pd$_4$@ZIF8-C(1173) immobilized AgPd nanoparticles were characterized by TEM (Fig. 4a and b)

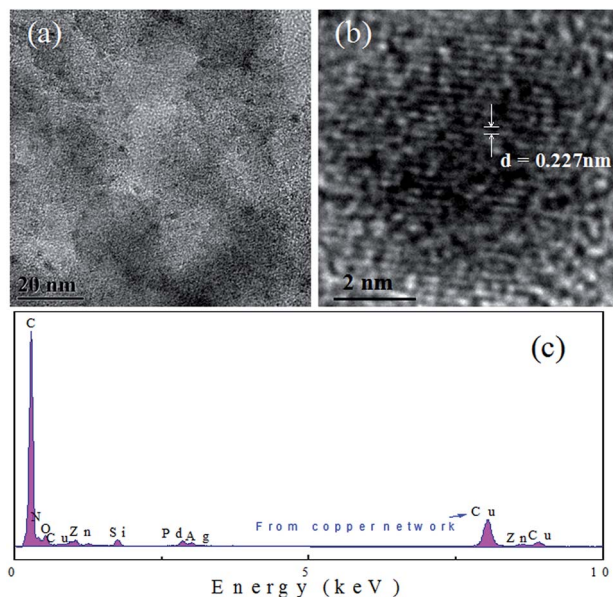and energy-dispersive X-ray spectroscopy (EDX) measurements (Fig. 4c). A representative high-resolution TEM image in Fig. 4b shows a *d*-spacing of 0.227 nm, which is between the (111) lattice spacing of face-centered cubic (fcc) Ag (0.24 nm) and Pd (0.22 nm), suggesting that Ag and Pd is formed as an alloy structure.[11] The mean diameter of AgPd nanoparticles in Ag$_1$-Pd$_4$@ZIF8-C(1173) was in the range of 5–8 nm (Fig. 4a), indicating AgPd nanoparticles was well dispersed on the surface of NPC.

Dehydrogenation of formic acid reaction

The catalytic dehydrogenation of formic acid has been performed over all the samples at 353 K in the presence of sodium formate (FA$_{mol}$: SF$_{mol}$ = 1 : 1) (Fig. 5). Catalytic performances of all the catalysts were studied based on the amount of gases measured volumetrically during the reaction. Their catalytic activities were strongly depended on the composition of AgPd clusters. The Ag$_5$@ZIF8-C(1173) was almost catalytic inactive. The catalytic activity increased while by alloying Pd and increasing the content of Pd. Ag$_1$Pd$_4$@ZIF8-C(1173) exhibits extremely high catalytic activity with the turnover frequency (TOF) value of 936 h^{-1} at 353 K. Further increasing the amount of Pd to Pd$_5$@ZIF8-C(1173) resulted in the decrease in catalytic activity, which highlighting the synergistic effect of molecular-scale AgPd alloy composition in ZIF8-C(1173) for the catalytic dehydrogenation of FA.

The influence of calcination temperature on the catalytic performance of the ZIF8-C(n) catalysts were investigated and the results were shown in Fig. 6. It can be seen that the volumen of H$_2$ and CO$_2$ catalyzed by Ag$_1$Pd$_4$@ZIF8-C(1173) reached its maximum in 5 minutes, which exceed the value of the other tested catalysts. The results clearly demonstrated that the best calcination temperature of ZIF-8 was 1173 K. Moreover, when the NPC ZIF8-C(1173) was treated by 10% HCl for 5 h to remove the zinc, a slightly lower hydrogen production rate was obtained with the Ag$_1$Pd$_4$@ZIF8-C(1073)-HCl catalyst. The results clearly demonstrated that the presence of Zn in NPC may be helpful to improve the dehydrogenation of FA.

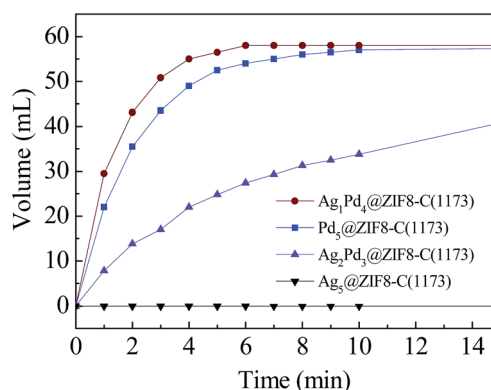**Fig. 4** TEM images of Ag$_1$Pd$_4$@ZIF8-C(1173) with different magnifications (a & b) and EDX spectrum of Ag$_1$Pd$_4$@ZIF8-C(1173) catalyst (c). The copper signal originates from Cu grid.

Fig. 5 Gas generation by decomposition of FA with different ratios of Ag/Pd supported on ZIF8-C(1173) *versus* time at 353 K ($n_{FA} = n_{SF} = 1.25$ mmol, $n_{metal} : n_{FA} = 0.01 : 1$).
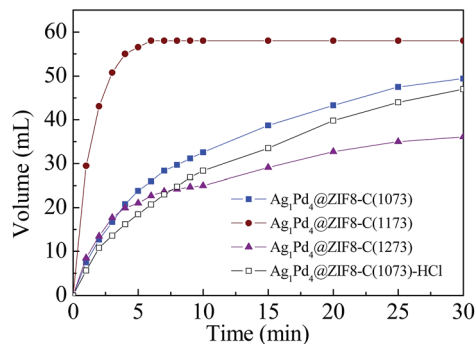
Fig. 6 Gas generation by decomposition of FA catalyzed by Ag_1-Pd_4@ZIF8-C(1073, 1173, 1273) and Ag_1Pd_4@ZIF(1073)-HCl catalysts at 353 K ($n_{FA} = n_{SF} = 1.25$ mmol, $n_{metal} : n_{FA} = 0.01 : 1$).

It is known that the decomposition of FA process can be improved by the addition sodium formate (SF) or NEt_3 *etc.*[1] We studied the hydrogen generation efficiencies of 1 : 1 (molar ratio) FA–SF, FA and SF solution catalyzed by Ag_1Pd_4@ZIF8-C(1173) at 353 K (Fig. 7). The results indicated that 1 : 1 FA–SF solution exhibits the highest hydrogen generation efficiency among the three solutions, the turnover frequency (TOF) value can be reached to 936 h^{-1}. For FA solution, the turnover frequency (TOF) value was 657 h^{-1}. Moreover, no gas was generated from pure SF solution.

Except H_2, the gas generated from the reaction was only CO_2 but no CO has been detected by gas chromatography analysis (Fig. S1 and S2,†), indicating the excellent H_2 selectivity for formic acid dehydrogenation catalyzed by Ag_1Pd_4@ZIF8-C(1173). To get the activation energy (E_a) of the dehydrogenation of FA catalyzed by Ag_1Pd_4@ZIF8-C(1173), the dehydrogenation reactions at different temperature ranging from 323 to 353 K were carried out. The TOF at different temperatures were calculated from the slope of the linear part of each plot from Fig. 8a. The Arrhenius plot of ln TOF *versus* $1/T$ for the catalyst was plotted in Fig. 8a, from which the obtained apparent E_a of the reaction was 23.6 kJ mol^{-1}, which is lower than the most reported values of E_a (Table 2).

Furthermore, We tested the recyclability of the Ag_1Pd_4@-ZIF8-C(1173) catalyst in the dehydrogenation of FA/SF at 353 K. The result showed that the as-synthesized catalysts could be
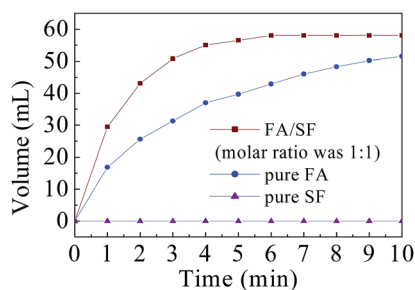

Fig. 7 Gas generation by decomposition of FA/SF *versus* time catalyzed by Ag_1Pd_4@ZIF8-C(1173) at 353 K ($n_{FA} = 1.25$ mmol, $n_{metal} : n_{FA} = 0.01 : 1$).
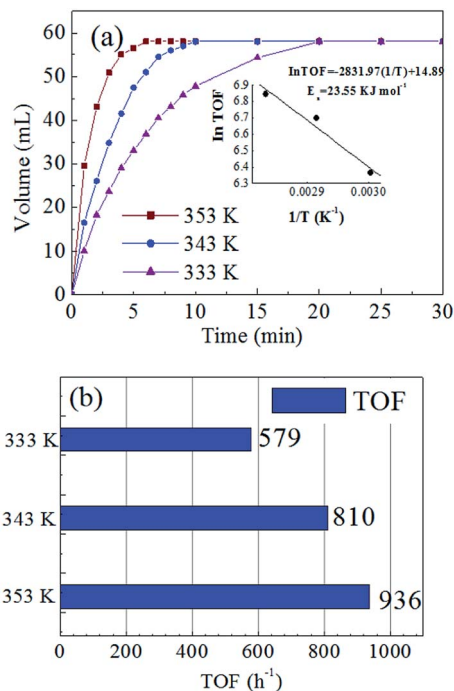

Fig. 8 (a) Volume of the generated gas ($CO_2 + H_2$) *versus* time and (b) corresponding TOF (calculated during the first 5 min of the reactions) values of H_2 generation for the dehydrogenation of FA/SF (1 : 1) at different temperatures over Ag_1Pd_4@ZIF8-C(1173). ($n_{FA} = n_{SF} = 1.25$ mmol, $n_{metal} : n_{FA} = 0.01 : 1$, and inset of (a): Arrhenius plot ln TOF *vs.* $1/T$).

reused for at least 5 runs without a significant loss of the catalytic activity (Table S2,†), suggesting that the catalyst has a quite good stability.

Table 2 Comparison of the activities of different catalysts for hydrogen generation from FA

Catalysts	T (K)	TOF (h^{-1})	E_a (kJ mol^{-1})	Ref.
Without additive				
Ag/Pd alloy	293	144		10
$Ag_{42}Pd_{58}$/C	323	382	22	11
$Co_{0.30}Au_{0.35}Pd_{0.35}$	298	80		29
$Au_{41}Pd_{59}$/C	323	230	28	30
Pd/C	323	30		30
$PtRuBiO_x$/C	353	312	37.3	33
AuPd–MnO_x/ZIF-8-rGO	298	382		35
With additive				
Ag_1Pd_4@ZIF8-C(1173)	353	936	23.6	This work
$Ag_{0.9}Pd_{4.2}$@ZIF-8	353	580	51.4	12
Pd–Au–Eu/C	365	387	84.2	27
AuPd@ED-MIL-101	363	106		28
$Ni_{18}Ag_{24}Pd_{58}$/C	323	85	20.5	31
Pd–Au/C	365	45	138.6	32
PdAu/C–CeO_2	365	113.5		32
Pd–S–SiO_2	358	719		34
$Ag_{0.1}$–$Pd_{0.9}$/rGO	298	105		36
PdNi@Pd/GNs-CB	RT^a	577		37

^{a} RT: room temperature.

Conclusions

In summary, we have demonstrated the fabrication of *in situ* NPC which feature high degree of graphitization, high surface area and hierarchical porosity by a facile low-cost and readily reproducible ZIF driven approach. The resultant NPC catalyst, Ag_1Pd_4@ZIF8-C(1173), exhibits high catalytic activity for the catalytic dehydrogenation of formic acid, with the turnover frequency (TOF) value of 936 h^{-1} and 100% hydrogen selectivity at 353 K. Our study reveals that solely ZIF-8 without additional nitrogen or carbon sources can be used as an ideal precursor to afford a NPC as catalyst carrier for decomposition of formic acid, the Zn and nitrogen derived from ZIF-8 nanocrystals can help to increase the dispersion of the AgPd alloy active species. With the great number of available and rapidly growing ZIF structures, ZIF-based NPC materials with tailorable pore textures and improved performances could be highly promising.

Acknowledgements

References

1 M. Grasemann and G. Laurenczy, *Energy Environ. Sci.*, 2012, **5**, 8171–8181.

2 Q. L. Zhu, N. Tsumori and Q. Xu, *Chem. Sci.*, 2014, **5**, 195–199.

3 A. Boddien, B. Loges, H. Junge and M. Beller, *ChemSusChem*, 2008, **1**, 751–758.

4 S. Fukuzumi, T. Kobayashi and T. Suenobu, *J. Am. Chem. Soc.*, 2010, **132**, 1496–1497.

5 A. Boddien, F. Gaertner, R. Jackstell, H. Junge, A. Spannenberg, W. Baumann, R. Ludwig and M. Beller, *Angew. Chem., Int. Ed.*, 2010, **49**, 8993–8996.

6 A. Boddien, D. Mellmann, F. Gaertner, R. Jackstell, H. Junge, P. J. Dyson, G. Laurenczy, R. Ludwig and M. Beller, *Science*, 2011, **333**, 1733–1736.

7 K. Jiang, K. Xu, S. Z. Zou and W. B. Cai, *J. Am. Chem. Soc.*, 2014, **136**, 4861–4864.

8 M. Ojeda and E. Iglesia, *Angew. Chem., Int. Ed.*, 2009, **48**, 4800–4803.

9 Z. L. Wang, H. L. Wang, J. M. Yan, Y. Ping, S.-I. O, S. J. Li and Q. Jiang, *Chem. Commun.*, 2014, **50**, 2732–2734.

10 K. Tedsree, T. Li, S. Jones, C. W. A. Chan, K. M. K. Yu, P. A. J. Bagot, E. A. Marquis, G. D. W. Smith and S. C. E. Tsang, *Nat. Nanotechnol.*, 2011, **6**, 302–307.

11 S. Zhang, Ö. Metin, D. Su and S. H. Sun, *Angew. Chem., Int. Ed.*, 2013, **52**, 3681–3684.

12 H. M. Dai, B. Q. Xi, L. Wen, C. Du, J. Su, W. Luo and G. Z. Cheng, *Appl. Catal., B*, 2015, **165**, 57–62.

13 H. M. Dai, N. Cao, L. Yang, J. Su, W. Luo and G. Z. Cheng, *J. Mater. Chem. A*, 2014, **2**, 11060–11064.

14 J. K. Sun and Q. Xu, *Energy Environ. Sci.*, 2014, **7**, 2071–2100.

15 W. Chaikittisilp, K. Ariga and Y. Yamauchi, *J. Mater. Chem. A*, 2013, **1**, 14–19.

16 L. Zhang, C. Feng, S. T. Gao, Z. Wang and C. Wang, *Catal. Commun.*, 2015, **61**, 21–25.

17 N. L. Torad, R. R. Salunkhe, Y. Q. Li, H. Hamoudi, M. Imura, Y. Sakka, C. C. Hu and Y. Yamauchi, *Chem.–Eur. J.*, 2014, **20**, 7895–7900.

18 Y. Y. Lu, W. W. Zhan, Y. He, Y. T. Wang, X. J. Kong, Q. Kuang, Z. Q. Xie and L. Zheng, *ACS Appl. Mater. Interfaces*, 2014, **6**, 4186–4195.

19 P. Zhang, F. Sun, Z. H. Xiang, Z. G. Shen, J. Yun and D. P. Cao, *Energy Environ. Sci.*, 2014, **7**, 442–450.

20 H. L. Jiang, B. Liu, Y. Q. Lan, K. Kuratani, T. Akita, H. Shioyama, F. Zong and Q. Xu, *J. Am. Chem. Soc.*, 2011, **133**, 11854–11857.

21 A. J. Amali, J. K. Sun and Q. Xu, *Chem. Commun.*, 2014, **50**, 1519–1522.

22 S. Lim, K. Suh, Y. Kim, M. Yoon, H. Park, D. N. Dybtsev and K. Kim, *Chem. Commun.*, 2012, **48**, 7447–7449.

23 Y. C. Zhang, L. G. Chen, G. Y. Bai, Y. Li and X. L. Yan, *J. Catal.*, 2005, **236**, 176–180.

24 Y. N. Zhang, Y. C. Zhang, C. Feng, C. J. Qiu, Y. L. Wen and J. Q. Zhao, *Catal. Commun.*, 2009, **10**, 1454–1458.

25 D. H. Kim, W. C. Lim, J. S. Park and T. Y. Seong, *J. Alloys Compd.*, 2014, **58**, 327–331.

26 L. J. Zhang, Z. X. Su, F. L. Jiang, L. L. Yang, J. J. Qian, Y. F. Zhou, W. M. Li and M. C. Hong, *Nanoscale*, 2014, **6**, 6590–6602.

27 X. Zhou, Y. Huang, C. Liu, J. Liao, T. Lu and W. Xing, *ChemSusChem*, 2010, **3**, 1379–1382.

28 X. Gu, Z. H. Lu, H. L. Jiang, T. Akita and Q. Xu, *J. Am. Chem. Soc.*, 2011, **133**, 11822–11825.

29 Z. L. Wang, J. M. Yan, Y. Ping, H. L. Wang, W. T. Zheng and Q. Jiang, *Angew. Chem., Int. Ed.*, 2013, **52**, 4406–4409.

30 Ö. Metin, X. Sun and S. Sun, *Nanoscale*, 2013, **5**, 910–912.

31 M. Yurderi, A. Bulut, M. Zahmakiran and M. G. Özkar, *Appl. Catal., B*, 2014, **160–161**, 514–524.

32 X. Zhou, Y. Huang, W. Xing, C. Liu, J. Liao and T. Lu, *Chem. Commun.*, 2008, 3540–3542.

33 S. W. Ting, S. Cheng, K. Y. Tsang, N. van der Laak and K. Y. Chan, *Chem. Commun.*, 2009, 7333–7335.

34 Y. Zhao, L. Deng, S. Y. Tang, D. M. Lai, B. Liao, Y. Fu and Q. X. Guo, *Energy Fuels*, 2011, **25**, 3693–3697.

35 J. M. Yan, Z. L. Wang, L. Gu, S. J. Li, H. L. Wang, W. T. Zheng and Q. Jiang, *Adv. Energy Mater.*, 2015, 1500107.

36 Y. Ping, J. M. Yan, Z. L. Wang, H. L. Wang and Q. Jiang, *J. Mater. Chem. A*, 2013, **1**, 12188–12191.

37 Y. L. Qin, J. Wang, F. Z. Meng, L. M. Wang and X. B. Zhang, *Chem. Commun.*, 2013, **49**, 10028–10030.